ANNALES
UNIVERSITATIS MARIAE CURIE-SKŁODOWSKA
LUBLIN – POLONIA
VOL. LXVI SECTIO AAA 2011

Mössbauer spectroscopy of iron-based superconductors

A. Błachowski[1], K. Ruebenbauer[1*], J. Żukrowski[2]

[1]Mössbauer Spectroscopy Division, Institute of Physics, Pedagogical University
PL-30-084 Cracow, ul. Podchorążych 2, Poland
[2]Solid State Physics Department, Faculty of Physics and Applied Computer Science,
AGH University of Science and Technology
PL-30-059 Cracow, Al. Mickiewicza 30, Poland

ABSTRACT

A brief review concerned with the application of the Mössbauer spectroscopy to the investigations of iron-based superconductors is given. An introduction is devoted to the description of the most important features of the Mössbauer spectroscopy followed by the discussion of the basic properties of iron-based superconductors. Our results obtained for FeSe, LiFeP and parent compounds of the '122' family, i.e., for AFe_2As_2 (A=Ca, Ba, Eu) are discussed later on with particular attention paid to the spin density wave (SDW) magnetism exhibited by the parents of the '122' family. It is found that incommensurate SDW contain many harmonics in these layered structures and evolve from almost separated magnetic sheets through *quasi*-triangular forms to almost rectangular shape with the lowered temperature.

1. INTRODUCTION

The Mössbauer spectroscopy is a typical shortsighted, i.e., a local nuclear method able to sample some local properties of the condensed matter [1, 2].

* Corresponding author. E-mail address: sfrueben@cyf-kr.edu.pl

The spectrum is sensitive to the hyperfine interactions between resonant nucleus and local electromagnetic fields. Due to the fact that two nuclear states are involved, i.e., the ground state and a resonant excited state one is able to see electron density on the resonant nucleus via the scalar contact electric interaction called isomer shift. No other nuclear methods sensitive to the hyperfine interactions have this property. In addition, one is able to see the electric quadrupole interaction between nuclear quadrupole moments (in both nuclear states provided nuclear spins are sufficiently high) and a local electric field gradient (EFG). Magnetic hyperfine interactions are seen in both nuclear states due to the dipolar interactions between nuclear magnetic moments and a local hyperfine field unless nuclear spins equal zero. For magnetically ordered systems a hyperfine field is a classical axial-vector field independent of time. There are numerous contributions to the hyperfine field generated mainly by the electronic magnetic moments. Dominant contributions are due to the electron/hole spin polarization, i.e. due to the local electron spin density. For strongly localized atomic magnetic moments one can expect large orbital contributions provided the electronic configuration is far away from the *S*-like states. For weakly coupled magnetic systems one can see a local coupling between electronic and nuclear moment in the paramagnetic state. The latter interaction quite often fluctuates on the time scale comparable to the inverse hyperfine frequency leading to the complex spectra called relaxation spectra. The Mössbauer spectroscopy has another unique feature within methods sensitive to the hyperfine interactions. It is able to see dynamics of the resonant atom in some limited way. Namely, a recoilless fraction, i.e. the probability of the resonant absorption depends on the time averaged second order and higher moments of the dynamic atomic displacement along the wave vector transfer to the system. Hence, it is similar to the corresponding factor important in the X-ray diffraction, albeit it differs in a subtle point that it does not depend on the static displacement in contrast to e.g. the X-ray diffraction and it is independent of the possible correlation in motion of different atoms. A mean squared velocity of the resonant atom is seen via the second order Doppler shift (SOD) as well. The SOD has some meaning at low temperatures as it reflects a zero-point motion. A classical equipartition principle makes it irrelevant for the solid state research at higher temperatures.

Spin density waves (SDW) are somewhat of a special kind of the electronic magnetic order due to the multi-particle phenomena [3]. They might lead to a periodic modulation of the electron spin density, i.e. to a periodic magnetization within the crystal space. A modulation is stationary and there-

fore one observes a static magnetization at a chosen lattice point. The origin of SDW could be traced to the presence of specific element within the crystal, but the magnetization due to SDW is de-localized except special cases of isolated impurities, the latter generating local damped electron spin oscillations around the impurity. Many possible kinds of order are possible within the SDW framework. The simplest SDW has all magnetic moments aligned in a plane, and it does not contain any constant component. Hence, the order of such a simple system is basically anti-ferromagnetic provided there are no other magnetic moments present. Surfaces of constant magnetization are generally planes parallel to one another, perpendicular to the "propagation" vector of SDW. A magnetization vector might have various orientations with respect to the propagation direction (except nodes, of course). Hence, one can observe longitudinal, perpendicular or mixed SDW depending on the system. The wavelength of SDW could be either commensurate with the lattice period along the propagation direction or not (incommensurate). Usually, the wavelength evolves with the temperature and/or pressure. The simplest SDW has strictly a sinusoidal shape along the propagation direction. However, higher odd multiplicities of the wave number are likely to make a significant contribution in many systems leading in the extreme case to the almost rectangular shape of SDW. Generally, SDW are likely to be the ground state of the electronic system provided the system behaves like metal and the Fermi surface is characterized by the presence of some nests/pockets capturing either electrons or holes. Layered systems with the reduced spatial dimensionality are more susceptible to this kind of order.

Mössbauer spectroscopy is very useful in studying the shape of SDW along the propagation direction provided the SDW is either incommensurate or the ratio of the SDW wavelength to the lattice period along the propagation direction is far away from the ratio of the small integers [4, 5]. Resonant atoms are located at some definitive positions in the chemical unit cell, while the SDW "slides" through these positions due to the incommensurate conditions even for the perfect system with completely coherent and unpinned SDW. The local magnetization generates a hyperfine field proportional to the fairly local amplitude of SDW via the core polarization mechanism. Mössbauer spectroscopy is unable to measure wavelength of the SDW, and it is unable to distinguish between coherent and incoherent state of SDW. A type of polarization is also hard to deduce from the Mössbauer spectra. Hence, the above properties are to be measured by some non-local method sensitive to the magnetic order like the neutron diffraction. On the other hand, the Mössbauer spectroscopy is unparalleled as far as the shape of SDW

is concerned as the neutron diffraction has limited sensitivity in the reciprocal space. One can be confident provided resonant atoms are main constituents of the material, and hence there are no additional effects of the spin oscillation due to the impurity effects. Some complication could be caused by the presence of other localized and ordered magnetic moments within material. One has to take into account the fact that usually the sign of the hyperfine field is inaccessible experimentally. The nuclear magnetic resonance is less useful as it requires application of the external fields, the latter being likely to perturb the SDW. Fig. 1 shows how the absorption spectrum with the single line unpolarized source is being built for the SDW having wave number q and propagating along direction x. This particular SDW is made of six subsequent odd harmonics and it is incommensurate. The hyperfine field B is generated by the above SDW. The presence of SDW leads to the characteristic hyperfine field distribution (distribution of absolute values) with integrable divergencies and subsequently to the spectrum shape shown as well in the transmission integral approximation. A transformation from the set of amplitudes through the SDW shape to the spectral shape is usually reversible and therefore numerically stable. On the other hand, a transformation from the SDW shape to the hyperfine field distribution is irreversible due to the presence of singularities. A transformation from the field distribution to the spectral shape is irreversible as well in the majority of cases. Hence, one cannot obtain the shape of SDW by adjusting field distribution, while the field distribution could be easily calculated from the shape of SDW the latter based directly on the spectral shape. Fig. 2 shows the evolution of the SDW-shape and evolution of the spectrum with addition of higher harmonics. Variation of the field distribution with addition of higher harmonics is illustrated as well.

The hyperfine Hamiltonian in the semi-classical approximation accessible via the Mössbauer spectroscopy leads to the eigenvalues and eigenvectors influencing the spectral shape. These eigenvalues and eigenvectors (in both nuclear states involved) depend in general on the following solid state parameters:

(1) the electron density on the nuclear site,
(2) the value of the total hyperfine magnetic field seen by the nucleus,
(3) the principal component of the EFG tensor on the nuclear site,
(4) the asymmetry parameter of the EFG tensor,
(5) polar and azimuthal angles between the hyperfine magnetic field and the principal axes of the EFG tensor.

Some additional information could be contained in the relative line intensities depending on the global orientation of the hyperfine field(s) with respect to the wave vector of the absorbed radiation.

A transition to the superconducting state is seldom observable by the Mössbauer spectroscopy, as the formation of the Cooper pairs and subsequent Bose condensate have no effect on the local hyperfine interactions. If some drastic change of the phonon density of states (DOS) occurs in correlation with the transition to the superconducting state one can see some spectra modification provided above change influences DOS projected on the resonant atom (PDOS). Such PDOS variation may have some influence on the recoilless fraction and SOD [6].

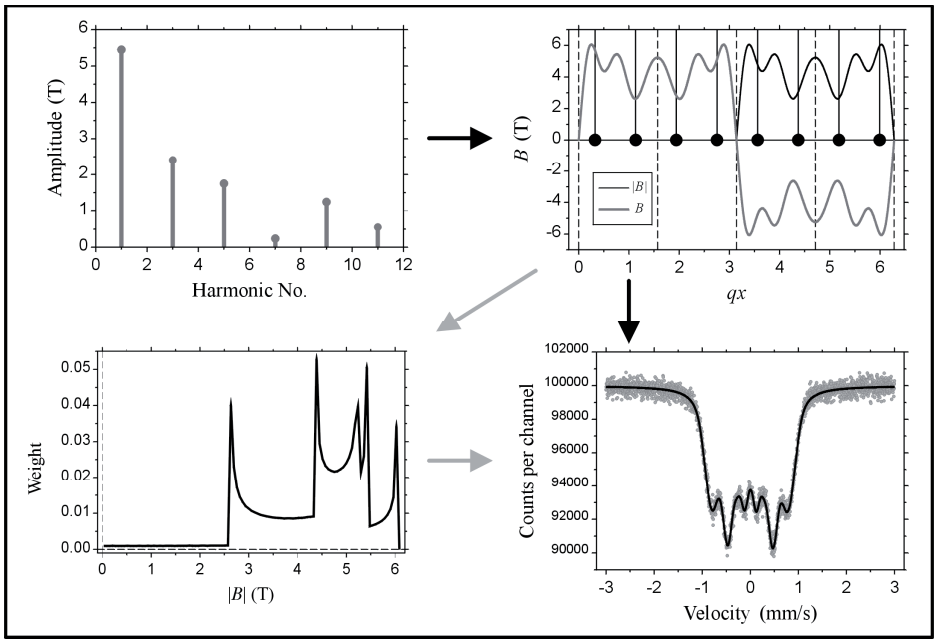

Fig. 1. Influence of SDW composed of harmonics having amplitudes shown in the upper left corner on the hyperfine field distribution (lower left corner) and spectrum shape (lower right corner) under incommensurate conditions (see upper right corner). A single row of sites accessible to the resonant atoms is shown in the upper right corner section. Light gray arrows mark generally irreversible transformations. Harmonics amplitudes are taken from Ref. [4] for $Ba(Fe_{1-x}Co_x)_2As_2$.

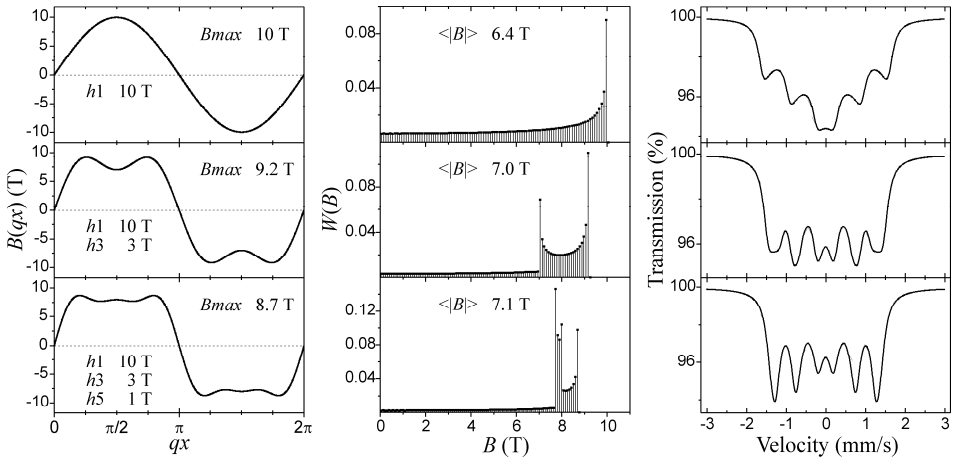

Fig. 2. Evolution of the SDW-shape, corresponding magnetic field distribution and shape of the Mössbauer spectra is shown versus addition of subsequent harmonics. The symbol qx stands for the phase of SDW, $W(B)$ denotes field distribution function plotted versus the field B. Maximum amplitudes of SDW B_{max} and amplitudes of the harmonics h_n ($n = 1, 3, 5$) are shown as well. The symbol $<|B|>$ denotes average of the respective distribution.

2. IRON-BASED SUPERCONDUCTORS

Iron-based superconductors are very similar in many aspects to cuprates, however some significant differences occur. We are going to limit current review to the layered iron pnictides and chalcogenides grouped in general into four families based on the magnetically ordered parent compounds having semi-metallic character of the electrical conductivity. Unit cells are tetragonal for all of these compounds. Some small orthorhombic distortion at low temperatures occurs in the most of cases [7-9].

The most complex family is denoted as '1111' and the parent compounds have the following composition LnFeAsO with Ln denoting rare earth atom like La, Ce, Pr, Nd, Sm, Gd, etc. A prototype unit cell of these compounds has the same crystallographic symmetry as the unit cell of SrFeAsF. Iron orders anti-ferromagnetically in the parent compounds forming longitudinal spin density wave having magnetic moment and propagation vector aligned with the a-axis. Iron atoms are arranged in planes perpendicular to the c-axis and they are surrounded by the As atoms forming nearly perfect tetrahedrons around iron atoms. Iron-arsenium layers resemble similar copper-oxygen layers in cuprates. However, they are not flat as in cuprates since As atoms are displaced

along the c-axis versus Fe atoms forming above tetrahedrons. Copper magnetic moments are oriented along <110> direction, while the moments due to the iron-induced SDW are oriented along <100> direction. Rare earth atoms make other planes perpendicular to the c-axis. Some of them (Ce, Nd, Sm, Gd, etc.) order magnetically at low temperatures as well. The superconducting state could be achieved by means of doping various atoms. The partial replacement of oxygen by fluorine leads to the superconductivity in the case of Ln=La, Sm. An oxygen deficient material in the case of Ln=Nd exhibits superconductivity as well. The partial replacement of Gd by Th leads to the superconducting state, too. The complete replacement of the arsenium by phosphorus and partial replacement of oxygen by fluorine results in the superconducting state for Ln=La. The SDW based magnetism diminishes with doping and eventually disappears just at the onset of the superconductivity as far as the ground state of the system is concerned. There are two iron-arsenium layers in the unit cell with iron located at c/4 and 3c/4 positions along the c-axis. They transform one into another by simple translation along the c-axis. Tab. 1 summarizes essential properties of the above compounds.

Parent compounds of the '122' family form almost perfect crystals of the composition AFe_2As_2 with A=Ca, Sr, Ba, Eu. There are again two iron-arsenium layers per unit cell at the same positions along the c-axis. However, they transform one into another by the translation along the c-axis and inversion in the iron plane. The SDW-type magnetism develops just below transition to the orthorhombic phase. Europium occurs in the divalent state and it orders magnetically at about 19 K forming ferromagnetic sheets perpendicular to the c-axis with the magnetic moments aligned along the a-axis. Subsequent sheets are ordered anti-ferromagnetically in the alternate fashion. The superconducting state could be achieved by substituting e.g. barium by potassium or rubidium, iron by cobalt or arsenium by phosphorus. Doping suppresses transition to the orthorhombic phase and leads to weakening of the SDW magnetism. Over-doped samples exhibit neither SDW magnetism nor superconductivity. There is some region of the dopant concentration, where superconductivity and SDW magnetism co-exist on the macroscopic scale. A magnetic ordering of the divalent europium seems to be completely insensitive to doping as far as the transition temperature is concerned. A similar conclusion could be reached for compounds of the '1111' family containing rare earth with a significant magnetic moment. Superconductivity could be achieved by applying external hydrostatic pressure to the parent compounds. Europium transforms into non-magnetic trivalent ion upon application of the pressure.

‘111’ family compounds consist of iron-arsenium or iron-phosphorus layers stacked by simple translation along the c-axis. It is essential to intercalate these layers by e.g. lithium in order to achieve the superconducting state. There is no magnetic order at all.

The simplest ‘11’ family is composed of either iron-selenium sheets or sheets with tellurium partly replaced by selenium or sulphur. Sheets are stacked by simple translation along the c-axis. A transition to the superconducting state could be increased for FeSe by doping with Te or by applying pressure. The superconductivity in FeSe is lost at very high pressure due to the transformation into the metallic, non-magnetic hexagonal phase. Usually, tetragonal FeSe metallic phase (orthorhombic at low temperature) co-exists with the hexagonal semiconductor having anti-ferromagnetic order of the high spin divalent iron ions. The latter phase undergoes spin re-orientation upon lowering temperature.

Tab. 1. Examples of the parent compounds and resulting superconductors obtained by doping. The symbol T_N stands for the magnetic transition temperature, the symbol μ denotes atomic magnetic moment, while the symbol T_S stands for the transition temperature to the superconducting state in the null external magnetic field. The symbol Fe refers to iron, while the symbol R to the rare earth with the magnetic moment [8, 9].

Family	Parent	T_N (K) Fe/R	μ (μ_B) Fe/R	Supercond.	T_S (K)
1111	LaFeAsO	137	0.4 – 0.7	$LaFeAsO_{0.89}F_{0.11}$	26
				$LaFePO_{1-x}F_x$	5
	CeFeAsO	140 / 4	0.8 / 0.8	$CeFeAsO_{0.85}$	46
	NdFeAsO	141 / 2	0.5 / 1.5	$NdFeAsO_{1-z}$	54
	SmFeAsO	130 / 2	0.4 / 0.6	$SmFeAsO_{1-x}F_x$	55
	GdFeAsO	133 / 4		$Gd_{0.8}Th_{0.2}FeAsO$	56
122	$CaFe_2As_2$	170	0.8	$CaFe_{1.92}Co_{0.08}As_2$	20
	$BaFe_2As_2$	140	0.9	$Ba_{0.6}K_{0.4}Fe_2As_2$	38
				$Ba_{0.7}Rb_{0.3}Fe_2As_2$	37
				$BaFe_2As_{1.3}P_{0.7}$	30
				$BaFe_{1.8}Co_{0.2}As_2$	23
	$EuFe_2As_2$	190 / 19	1.0 / 5.9	$Eu_{0.5}K_{0.5}Fe_2As_2$	32
				$Eu_2Fe_{2-x}Co_xAs_2$	10
				KFe_2As_2	4
111				LiFeAs	18
				LiFeP	6
11	$Fe_{1.1}Te$	70	2.2	$FeTe_{0.6}Se_{0.4}$	15
				FeSe	8

3. SELECTED RESULTS

3.1. IRON SELENIDE OF THE '11' FAMILY

The sample was prepared by direct solid state reaction between iron and selenium. The formal stoichiometry was chosen as $Fe_{1.05}Se$ [10]. The final step of the synthesis was performed as the sample annealing at 1023 K with subsequent rapid quench in order to avoid as much as possible the formation of the δ-FeSe hexagonal phase. A dominant phase is the required β-FeSe tetragonal phase with some minor phases like δ-FeSe of the Fe_7Se_8 type with the defect order pattern of the *3c* kind, Fe_3O_4 and α-Fe present. Fortunately all these minor phases are already magnetically ordered at room temperature, and therefore their contributions to the Mössbauer spectra could be easily separated from the contribution due to the β-FeSe.

A magnetic susceptibility measured versus temperature is shown in Fig. 3. The pelletized sample was cooled in the zero external field to 2 K and subsequently warmed up to 355 K in the applied field of 5 Oe. Afterwards the susceptibility was measured in the sweep mode upon cooling sample to 2 K in the field of 5 Oe, and subsequent warming in the same field up to 305 K. The region marked **A** is due to the spin re-orientation in the insulating hexagonal phase δ-FeSe. The Vervey transition in magnetite does not show up here, but it is clearly seen in the Mössbauer spectra obtained for the high velocity range. A broad maximum marked **B** is caused by a transition from the tetragonal to the orthorhombic structure within the major phase. The origin of this exceptional increase of the susceptibility (magnetic anomaly) remains unexplained. Finally a transition to the superconducting state is seen around region marked **C**. The susceptibility remains positive in the superconducting state due to the presence of the ferromagnetic minor phases – mainly α-Fe.

Mössbauer spectra collected versus temperature at low velocity range are shown in Fig. 4. There is no change in the quadrupole interaction upon transformation from the tetragonal to the orthorhombic phase. A transition to the superconducting state makes no mark on the spectra. The major effect is the SOD varying with the temperature.

However, a transition from the tetragonal to the orthorhombic phase is accompanied by a small, albeit significant jump in the isomer shift by +0.006(1) mm/s corresponding to the change of the electron density on the iron nucleus by – 0.02 electron a.u.$^{-3}$ according to the recently determined calibration constant for this transition [11]. Fig. 5 shows the above jump in the isomer shift.

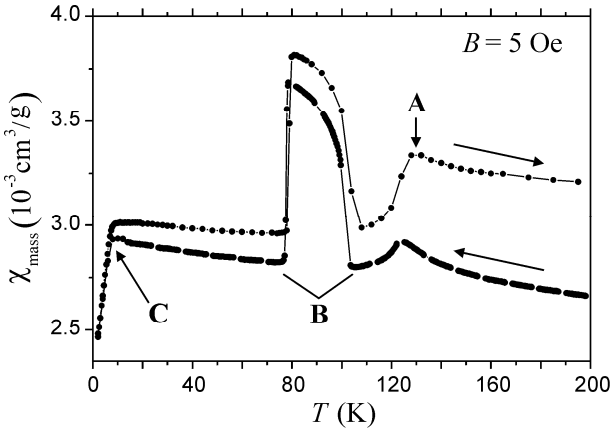

Fig. 3. Magnetic susceptibility measured versus temperature T upon cooling and subsequent warming of the sample. Applied field B is well below the first critical field.

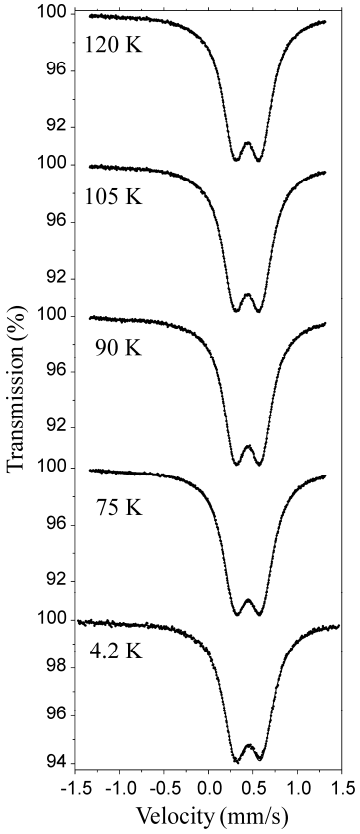

Fig. 4. Mössbauer spectra versus temperature obtained in the null external magnetic field. Spectra were collected for the low velocity range.

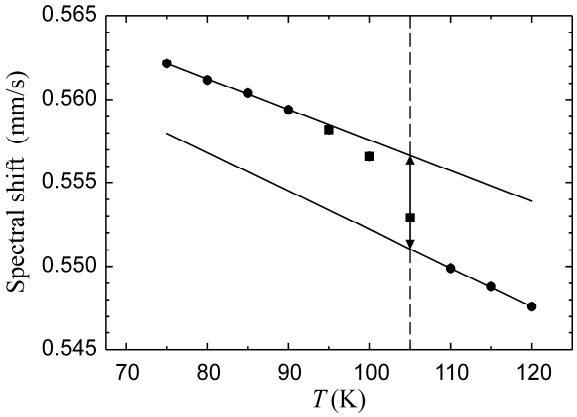

Fig. 5. Spectral-shift versus temperature in the phase transition region. The shift scale is calibrated versus shift of the α-Fe at room temperature and ambient pressure. Points marked by rectangles are excluded from respective linear regression fits representing variation of SOD in the narrow temperature ranges. Note departure of SOD from the classical high temperature limit within the temperature region shown – seen as slightly bigger slope of the line fitted to the high temperature points in comparison with similar slope of the line fitted to the low temperature points.

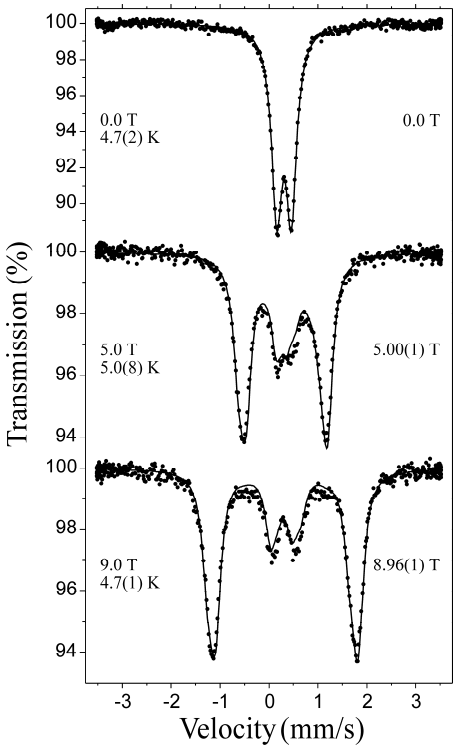

Finally, the spectra obtained in the strong external magnetic field oriented along the radiation beam are shown in Fig. 6. A standard ^{57}Co(Rh) source was kept out of the field and at the sample temperature (for all measurements without external field the source is kept at room temperature). Note that the field acting on the iron nucleus is practically an applied field despite low temperature

Fig. 6. Spectra obtained in the external magnetic field co-axial with the radiation beam. The source was kept at the same temperature as the absorber, albeit in the null external field. The middle spectrum was obtained for the field of 5 T, while the lower spectrum for the field of 9 T. Values shown on the right part of the middle and lower plots represent fields acting on the iron nuclei – derived from fits to the data.

of the sample. Hence, one can conclude that the sample is either diamagnetic or exhibits the Pauli type of paramagnetism. These spectra show as well that the EFG tensor is axially symmetric with the negative principal component having maximum absolute value. Such behavior is expected for the iron-selenium layers forming nearly perfect tetrahedron around the iron atom. One can conclude that above principal component of the EFG tensor is parallel to the tetragonal (orthorhombic) axis. Applied fields of 5 T and 9 T are higher than the first critical field at the sample temperature (5.0(8) K for field of 5 T and 4.7(1) K for 9 T), but much lower than the second critical field. On the other hand, there is no visible component with either reduced or absent field in both cases. Hence, one can conclude that at least 99 % of the sample volume is penetrated by the external field in whole - leaving very small, albeit very important superconducting volume.

3.2. LIFEP OF THE '111' FAMILY

The sample was prepared by the solid state reaction between components under reducing atmosphere and in the gold container. It was slightly contaminated by FeP (complex magnetic ordering at about 115 K) and Fe_2P (ferromagnetic ordering at about 215 K). Magnetization measurements show a transition to the superconducting state at 5.5 K [12]. On the other hand, the second critical field was found to lie between 0.1 T and 0.5 T. Mössbauer spectra are shown in Fig. 7 versus temperature. The main component is characterized by a relatively broad quadrupole split doublet with the splitting slightly increasing upon lowering temperature. Lines are broad due to the lithium disorder. They are becoming

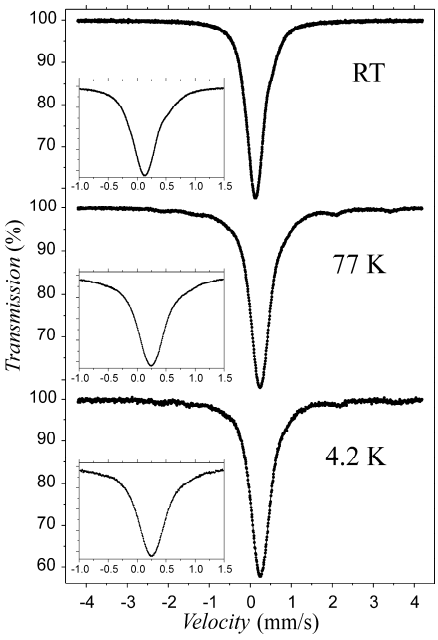

Fig. 7. Spectra of LiFeP are shown versus temperature. Insets show expanded velocity scale with the contribution from the LiFeP phase. Minor phases order magnetically between room temperature and liquid nitrogen temperature.

narrower close to room temperature probably owing to the significant lithium mobility at higher temperatures. No magnetic ordering occurs.

3.3. COMPOUNDS OF THE '122' FAMILY

Parent compounds of this family have the following chemical formula AFe_2As_2 with A=Ca, Sr, Ba, Eu. Detailed investigations have been performed for all of the above compounds except for the strontium-based system. A transition from the tetragonal to the orthorhombic unit cell occurs upon lowering temperature and it is characterized by the narrow hysteresis loop. The electron density on the iron nucleus slightly increases upon transformation to the orthorhombic phase in contrast to the corresponding decrease in the FeSe system. The SDW-type magnetic order develops just below transition to the orthorhombic phase [13]. The SDW has a magnetic field aligned with the a-axis and it has longitudinal character. The SDW is incommensurate with the lattice period along the a-axis. There is no transition to the superconducting state. Europium remains in the form of divalent $^8S_{7/2}$ ion and it orders magnetically at about 19 K forming alternating ferromagnetic sheets perpendicular to the c-axis with the Eu magnetic moments oriented along the a-axis. The EFG tensor is axially symmetric on iron and europium with the principal component oriented along the c-axis in both cases. The principal component is negative on Fe and Eu both. Fig. 8 shows evolution of the SDW versus temperature in $EuFe_2As_2$ as derived from the spectra by using GMFPHARM application of the MOSGRAF-2009 software suite [14].

The square root from the mean squared amplitude of the SDW $\sqrt{<B^2>}$ is plotted versus temperature in Fig. 9 for all compounds investigated. There are two distinct temperature regions as far as the kind of magnetic order is considered. The low temperature region is characterized by the power law behavior with the critical exponent indicating $(1,2)$ universality class, i.e., the one dimension of the spin space (Ising-like behavior of spins) and two dimensions in the configuration space (strongly planar character of the magnetic ordering). The critical exponents were found as 0.158(2) for $CaFe_2As_2$, 0.102(1) for $BaFe_2As_2$ and 0.124(1) for $EuFe_2As_2$ in comparison with the ideal value of $\frac{1}{8}$. They are somewhat underestimated due to the presence of the "tail" at higher temperatures.

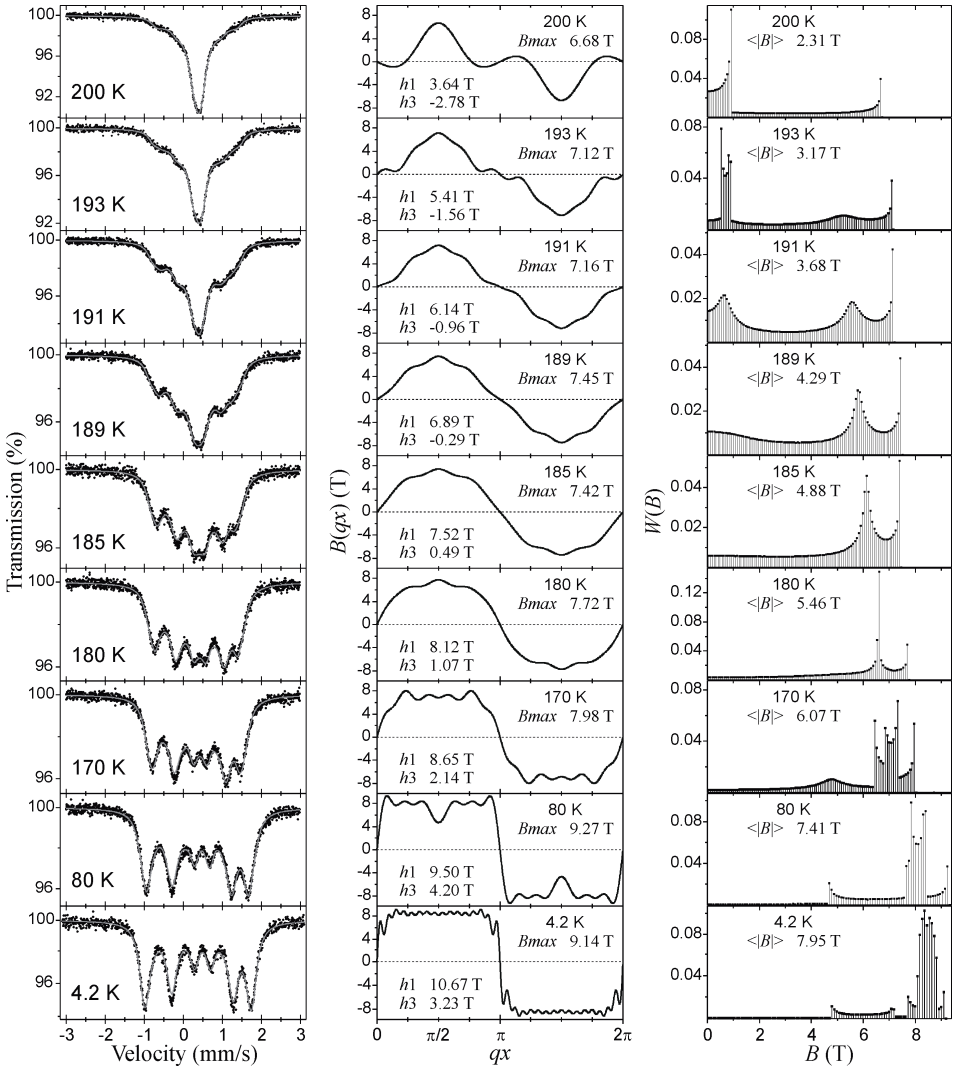

Fig. 8. Evolution of the SDW shape in $EuFe_2As_2$ versus temperature. The left column shows spectra, the central column shows the corresponding shape of SDW versus the phase of SDW marked as qx, while the right column shows resulting field distribution $W(B)$ plotted versus the field B. Maximum amplitudes of SDW B_{max} and amplitudes of the first two harmonics h_1 and h_3 are shown as well. The symbol $<|B|>$ denotes average of the respective distribution.

The second region ("tail") is due to the incoherent SDW developing from the coherent SDW of the low temperature described previously region. The second region extends till the transition to the tetragonal phase. It is go-

verned by the power law expressed as $(T/T_c)^{-\beta}$ with the exponent β strongly correlated to the coupling between magnetic planes, i.e., to the lattice constant along the c-axis. The exponent β varies from 3.8(1) for $CaFe_2As_2$, with the smallest lattice constant to 20.4(4) for $BaFe_2As_2$, with the largest lattice constant. Transition temperatures T_c are found as 175.3(3) K for $CaFe_2As_2$, 136.0(1) K for $BaFe_2As_2$ and 192.1(1) K for $EuFe_2As_2$. They are defined as temperatures, where the coherent SDW vanishes. Magnetic ordering of europium is invisible by the iron-based SDW, and therefore there is no transferred field from Eu to Fe atoms. The absence of the transferred field from Eu on the Fe positions means that iron atoms see the europium filled layers rather like uniformly magnetized planes than individual atoms despite localized character of the europium 4f magnetic moment resulting from the $^8S_{7/2}$ electronic configuration.

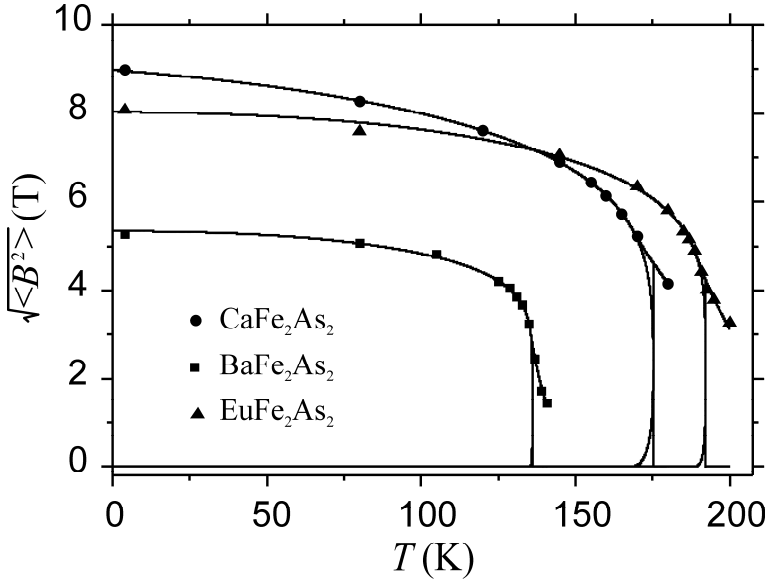

Fig. 9. Plot of square root from the mean squared amplitude of SDW $\sqrt{< B^2 >}$ versus temperature. Solid lines represent total, coherent, and incoherent contributions.

4. CONCLUSIONS

The basic conclusions could be summarized in the following way as far as the Mössbauer spectroscopy is concerned in the context of the application

to the solid state problems – in particular, to the investigation of the iron-based superconductors.

1. Variation of the electron density and electric field gradient on the resonant nucleus due to the phase transition is generally seen via the variation of the isomer shift and variation of the quadrupole interaction.
2. Measurements at low temperature and in the strong external magnetic field are able to detect even very small electronic magnetic moment on the resonant nucleus.
3. The Mössbauer spectroscopy is very sensitive to the shape of the spin density waves, and hence evolution of the SDW shape versus temperature could be studied quite accurately.
4. The direction of the hyperfine field could be deduced basing on the relative orientation of the hyperfine field and the electric field gradient, the latter having definite orientation in the crystal cell.

On the other hand, iron-based superconductors seem very interesting materials from the point of view of the basic science, as they exhibit complex interplay between magnetic order and superconductivity. There is no evidence that Cooper pairs are coupled by some other mechanism than the phonon mechanism, but the 3d magnetism appears close to the superconducting state and slight variation of the electron band due to doping and/or pressure transforms the system from one to another state. Parents of the iron-based superconductors exhibit typical itinerant magnetism appearing as SDW with the period incommensurate with the lattice periodicity. The shape of SDW is far from the simple sinusoidal shape.

ACKNOWLEDGMENTS

Zbigniew Bukowski (ETH–Zürich and INTiBS–PAN–Wrocław), Janusz Karpinski (ETH–Zürich), Jacek Marzec (AGH–Cracow), Janusz Przewoźnik (AGH–Cracow), Krzysztof Rogacki (INTiBS–PAN–Wrocław), Zbigniew M. Stadnik (U. Ottawa), and Krzysztof Wojciechowski (AGH–Cracow) are warmly thanked for fruitful co-operation during studies of the iron-based superconductors.

REFERENCES

[1] R.L. Mössbauer, Z. Physik, **151**, 124 (1958)
[2] P. Gütlich, E. Bill and A.X. Trautwein, *Mössbauer Spectroscopy and Transition Metal Chemistry*, Springer Verlag (2010).
[3] A.W. Overhauser, Phys. Rev., **128**, 1437 (1962)
[4] P. Bonville, F. Rullier-Albenque, D. Colson and A.Forget, EPL, **89**, 67008 (2010)
[5] J. Cieślak, Ph.D. Thesis, AGH University of Science and Technology, Cracow, Poland, 1995; J. Cieślak and S.M. Dubiel, Nucl. Instrum. Methods B, **95**, 131 (1995)
[6] J. Lindén, J.-P. Libäck, M. Karpinnen, E.-L. Rautama and H. Yamauchi, Solid State Commun., **151**, 130 (2011)
[7] Y. Kamihara, T. Watanabe, M. Hirano and H. Hosono, J. Am. Chem. Soc., **130**, 3296 (2008)
[8] D.C. Johnston, Adv. Phys., **59**, 803 (2010)
[9] M.D. Lumsden and A.D. Christianson, J. Phys.: Condens. Matter, **22**, 203203 (2010)
[10] A. Błachowski, K. Ruebenbauer, J. Żukrowski, J. Przewoźnik, K. Wojciechowski and Z.M. Stadnik, J. Alloys Compd., **494**, 1 (2010)
[11] U.D. Wdowik and K. Ruebenbauer, Phys. Rev. B, **76**, 155118 (2007)
[12] A. Błachowski, K. Ruebenbauer, J. Żukrowski, J. Przewoźnik and J. Marzec, J. Alloys Compd., **505**, L35 (2010)
[13] A. Błachowski, K. Ruebenbauer, J. Żukrowski, K. Rogacki, Z. Bukowski and J. Karpinski, Phys. Rev. B, **83**, 134410 (2011)
[14] K. Ruebenbauer and Ł. Duraj: www.elektron.up.krakow.pl/mosgraf-2009